An Unconventional Shape Memory Alloy Low-Power Ratchet for Reconfiguring the Polarization of a Moiré Pattern-Based Antenna

Joe Taoum, Elie Shammas, *Senior Member, IEEE*, and Joseph Costantine, *Senior Member, IEEE*

***Abstract*— In this article, a novel polarization reconfigurable antenna based on the Moiré effect is proposed. The presented design exploits substantial changes in the overlapped Moiré patterns to minimize the needed actuation for antenna reconfiguration. The novel antenna design is based on stacking two circular FR4 substrates on top of a truncated edge rectangular patch antenna. The top layers of both the substrates are milled into horizontal stripes forming the Moiré patterns. One of these substrates is fixed with respect to the antenna, while the second one rotates with respect to the fixed substrate. Upon rotation, these stripes from the two substrates overlap in pattern, which shapes the antenna. As a result, the antenna design is capable of switching its polarization scheme between vertical, horizontal, and circular with left-hand orientation. In addition, the Moiré patterns can also enhance the directivity and gain of the proposed antenna. The reconfiguration's mechanical actuation is achieved via a nontraditional ratchet mechanism that uses shape memory alloys (SMAs). This realized actuation system is fast, flexible in its positioning, has low energy expenditure, and minimizes interference with antenna operation. An antenna prototype is fabricated and tested where measured results match the simulated performance.**

***Index Terms*— Mechanical actuation, Moiré patterns, polarization reconfiguration, ratchet mechanism, reconfigurable antennas, shape memory alloys (SMAs).**

I. Introduction

RECONFIGURABLE antennas constitute the next frontier in agile and dynamic communication needs. Such communication schemes that extend beyond advances in terrestrial communications toward space communications promise to provide flexibility in operation and the ability to cater for any arising situation. Reconfigurable antennas in general are advantageous due to their capability to change their radiation characteristics intentionally and on demand. As a result, one antenna can morph its topology through the implementation of various reconfiguration components from one state into another to reconfigure its operation. A common method to modify the characteristics of an antenna is through mechanical reconfiguration. For example, the operating frequency of a helical antenna can be tuned by mounting it to a height-adjustable origami structure [1] or by physically changing the number of turns of the helix using movable arms' guides inside hollow helical tubes [2]. Another design relies on soft robotics, where an inflatable pneumatic structure carrying copper strips acts as a monopole [3]. On the other hand, placing movable parasitic patches or rotating metasurfaces on top of an antenna was successful in changing the antenna's operational frequencies [4] and [5]. The idea of metasurfaces was also explored to achieve beam steering capabilities [6]. Similar to metasurfaces, the beam of an antenna array was steered by rotating a stack of aluminum layers, acting as waveguides, with respect to an antenna array [7]. Another approach leveraged liquid metal to design a director and a reflector to steer the radiating beam [8]. In addition, the antenna's radiation pattern was physically reconfigured by replacing the ground plane of the antenna by a rotating anisotropic carbon fiber plane [9], or by inserting shorting screws between the patch antenna and its ground [10]. As for polarization reconfiguration, a circularly polarized patch antenna was designed to change from left-hand circular polarization (LHCP) to right-hand circular polarization (RHCP) by manually rotating it about a fixed feeding point [11].

In addition to mechanical reconfiguration, several switching or tuning methods rely on electronic components such as PIN diodes [12], [13], varactors [14]–[16], or microelectromechanical (MEMS) switches [17], [18]. Due to their electrical nature, these techniques present many challenges despite their fast response. The dc biasing current required for these switches must be carefully designed not to interfere with the antenna performance [5], [19].

Another important factor in designing mechanically reconfigurable antennas is the type of actuators used. Ideally, an actuator should be reliable, provide fast reconfiguration, have low power consumption, and does not interfere with the antenna's radiation. While the most common types of actuators

Manuscript received 10 August 2021; revised 22 April 2022; accepted 19 June 2022. Date of publication 7 July 2022; date of current version 17 November 2022. This work was supported by the American University of Beirut (AUB), University Research Board (URB). *(Corresponding author: Joseph Costantine.)*

Joe Taoum and Elie Shammas are with the Mechanical Engineering Department, American University of Beirut, Beirut 1107 2020, Lebanon (e-mail: es34@aub.edu.lb).

Joseph Costantine is with the Electrical and Computer Engineering Department, American University of Beirut, Beirut 1107 2020, Lebanon (e-mail: jcostantine@ieee.org).

Color versions of one or more figures in this article are available at https://doi.org/10.1109/TAP.2022.3187509.

Digital Object Identifier 10.1109/TAP.2022.3187509

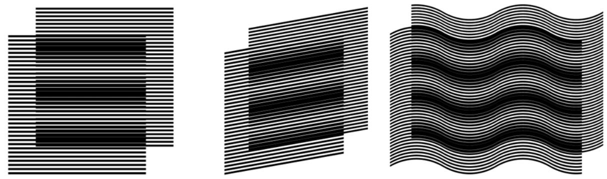

(a) (b) (c)

Fig. 1. Typical examples of Moiré stacking using (a) horizontal lines, (b) inclined lines, and (c) curves [25].

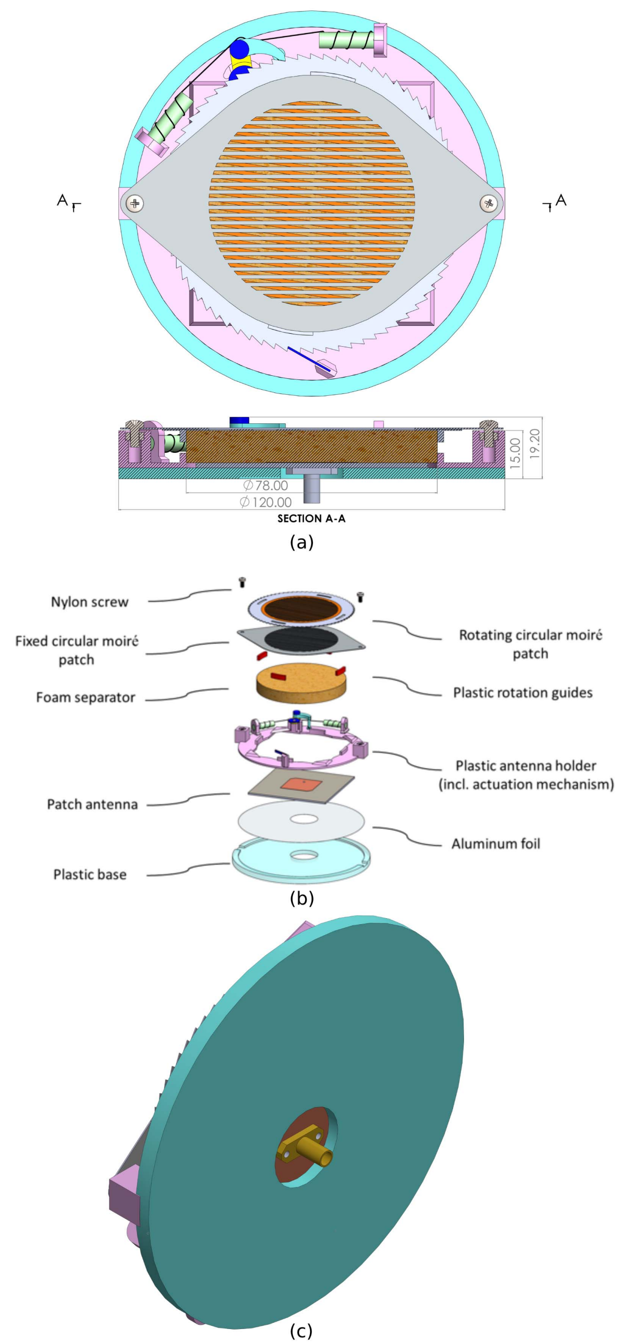

Fig. 2. CAD representation of the proposed reconfigurable antenna seen as (a) top view along its cross-sectional view, (b) exploded view, and (c) bottom perspective view showing the antenna's feed.

are dc motors with all their variations (e.g., stepper motors, servo motors) [2], [4], [6], [10], [20], [21], telescopic actuators have also been used for linear motion [1], [22].

Furthermore, pumps have been implemented in mechanisms containing liquid metals or other fluids, as seen in [3] and [8]. On the other hand, more recent actuating mechanisms such as shape memory alloys (SMAs) to adjust the height of a helical antenna or piezoelectric actuators (PZT) have been discussed in [23] and [24].

In this article, a novel mechanically reconfigurable antenna with low actuation energy consumption is developed. The reconfiguration is possible by rotating two overlaying conductive layers to create the Moiré effect. Generally, Moiré patterns are obtained by superposing two layers with similar patterns. The minimal relative displacement between these layers produces new opaque shapes. The two layers are commonly divided into a "base layer" and a "revealing layer," as shown in Fig. 1 [25]. Due to its high sensitivity to displacements, the Moiré effect is useful for many applications, such as strain analysis [26] or document counterfeiting [27].

For the proposed antenna design, two copper layers with horizontal line patterns are superimposed and rotated with respect to each other on top of a patch antenna. The produced Moiré effect changes the spatial density of the "grid" created by the two layers of copper, which affects the radiation characteristics of the antenna. The small increments' rotation of the patches is achieved by a ratchet mechanism and an SMA actuator, which can be operated on a minimal power budget.

Hence, the novelty of the work presented in this article is based on its polarization diversity, which is possible by relying on small rotation angles only. Combined with a low energy actuation mechanism, the Moiré effect from the FR4 substrates reconfigures the proposed antenna system's polarization from linear to circular.

In this article, Section II examines the design of the structure's parts and assembly, along with the mechanical actuation system that consists of a ratchet mechanism driven by two SMA actuators. Section III presents the antenna's performance by displaying the simulated and experimental work. Section IV concludes the article.

II. Reconfigurable Antenna Design

A. Antenna Structure

The assembly of the proposed antenna, as shown in Fig. 2, consists of the Moiré substrates, the driven antenna, the actuation mechanism, and the supporting structure. Each Moiré patch is composed of a 0.4 mm FR4 substrate that is copper cladded on one side only. Within a circle of 64 mm diameter from the center of each patch, horizontal stripes of 1.2 mm width and 1.2 mm separation distance are milled using a mechanical computer numerical control (CNC) machine. The width and separation distance of the horizontal stripes on the Moiré substrates are chosen to be around one hundredth of the driven antenna's wavelength $\lambda/100$ mm, where λ is 122 mm.

The outer shape of the fixed top substrate is laser cut and fixed to the supporting structure via two nylon M3 screws.

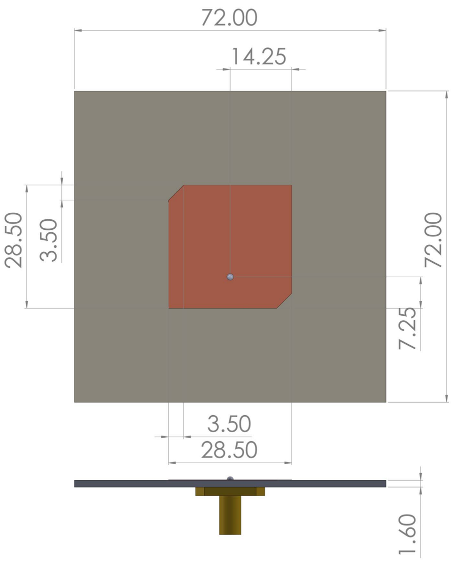

Fig. 3. Base antenna dimensions.

The rotating patch has outer teeth laser cut on its boundary which will be used for the ratcheting mechanism. The ratchet teeth are designed to allow 5° rotation increments over the full 360° range. The base antenna, a truncated edge rectangular patch, as shown in Fig. 3, is designed to operate at 2.45 GHz with an LHCP and is placed 10 mm below the copper layers.

The plastic base and plastic antenna holder are 3-D-printed using polyactic acid (PLA) as the printing material with 10% infill (90% hollow inside). According to the measurements done in [28], the infill percentage has great impact on the permittivity. When reducing the infill from 100% to 10%, the relative permittivity of PLA decreases from 3.4 to less than 1.8, making it ideal for the proposed antenna application. Another important aspect in the design is the thin thickness of the parts, where the plastic base, antenna holder, and Moiré patches are of 5, 1.6, and 0.4 mm, respectively. A computer-aided design (CAD) drawing showing the individual components is presented in Fig. 4.

In addition to the plastic parts, a circular Styrofoam is placed between the top of the antenna patch and the bottom layer of the first substrate as a guide for rotation, and to provide the 10 mm separation distance between the base antenna and the Moiré patches. The two screws and nuts holding the top patch are made of nylon instead of steel, in the same effort of minimizing interferences. Finally, a circular aluminum foil is placed in contact with the base antenna's ground to enhance the overall ground plane of the proposed antenna. Fig. 5 shows the fabricated prototype of the proposed antenna.

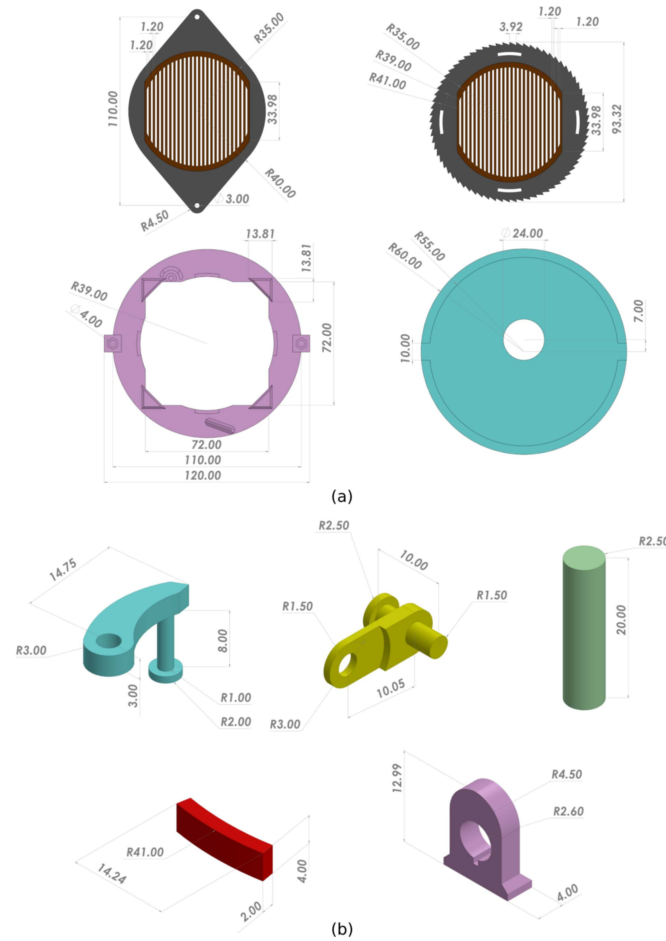

Fig. 4. CAD representations of (a) major components of the antenna and (b) minor components of the proposed antenna.

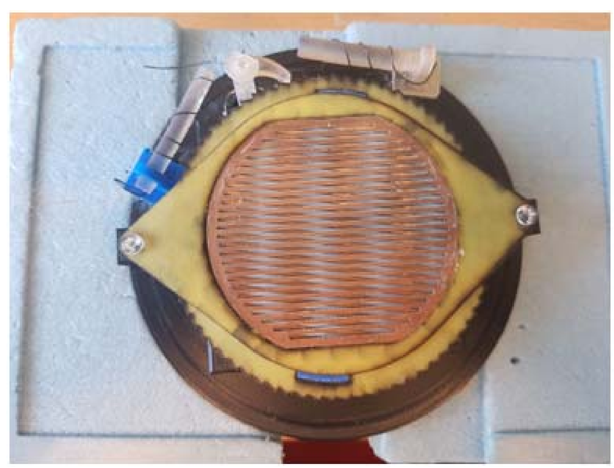

Fig. 5. Fabricated antenna prototype.

B. Actuation Mechanism

The actuation choice for the proposed design is SMAs coupled with the mechanical ratcheting mechanism. This choice is guided by the low power consideration and minimal RF interference.

SMAs are materials that exhibit shape memory and pseudo elastic effects. These interesting phenomena allow designers to use SMA wires as actuators. Using the shape memory effect, SMA wires can be trained to different shapes such as springs that return to their initial shapes upon heating above a transition temperature. On the other hand, a straight SMA

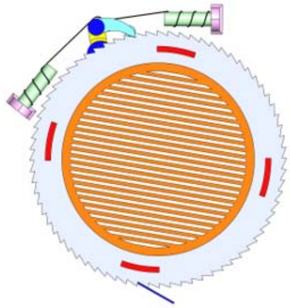

(a)

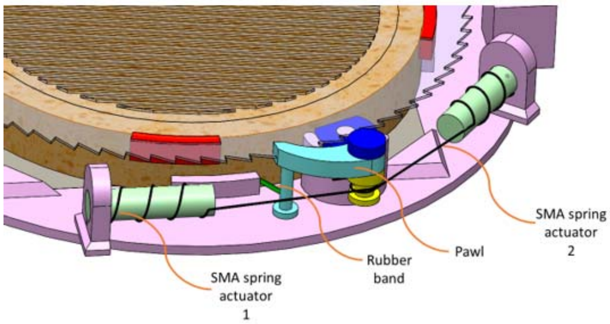

(b)

Fig. 6. CAD representation of the proposed actuation mechanism as (a) top view and (b) annotated perspective view.

Fig. 7. Actuation mechanism used in the prototype.

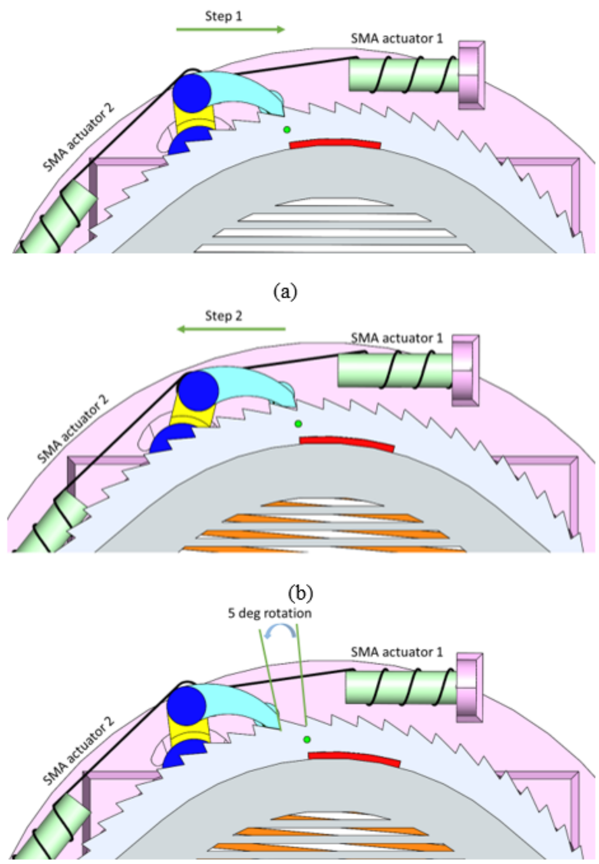

(a)

(b)

(c)

Fig. 8. CAD representation of the proposed actuation mechanism during (a) the activation of SMA actuator 1, (b) the activation of SMA actuator 2, and (c) the end result of a 5° rotation.

wire can also be used as an actuator by relying on the pseudo elastic effects, where the wire can be effectively contracted by more than 3% of its original length when heated [29]. While an SMA wire actuator produces more force, a spring-shaped SMA enables a larger stroke with smaller forces. Their low weight, along with their high energy density and shape versatility, renders them a suitable competitor for the more traditional actuators such as dc [30]. SMA actuators have many applications in the robotic, biomedical, and aerospace industries [31]. They are also typically used in deployable structures for satellite antennas [32] or for repositioning a reconfigurable helical antenna [23].

The typical disadvantages of SMAs, such as their high temperature requirements and nonprecise positioning due to their hysteresis loop [33], are overcome by properly designing the proposed ratchet mechanism. For the proposed design, a 0.02” (0.508 mm) shape memory Nitinol (nickel–titanium alloy) wire is used. The helical spring shape of the SMA is obtained by winding the wire around a 6 mm screw and firmly fixing both ends using two nuts. The setup is then heated in an oven at 500 °C for 50 min to train the wire. The final step is to quench the wire in cool water. As a result, the previously straight wire develops a new helical shape. Upon the application of heat to the deformed spring shape, typically using an electric current, the spring returns to its initial unstretched shape.

The proposed actuation system, represented by the ratchet mechanism and two SMA actuators, is shown in Figs. 6 and 7. A conventional ratchet mechanism typically consists of two pawls and at least two metallic springs. In the proposed mechanism, a rubber band replaces the first metallic spring, whereas a compliant plastic rod, shown as rectangular blue rod in Fig. 6(a), replaces the second pawl and its spring. The design tends to minimize the presence of metallic parts in the actuation system of the antenna.

In Fig. 8, the pawl is in contact with the teethed disk and is attached to the two SMA helical springs. When an electric current is applied through SMA spring actuator 1, the spring contracts by less than 10 mm, moving the pawl and the teethed disk by 5°. The precise 5° rotation is guaranteed by mechanical stops, which do not allow the pawl to travel further distances. At this stage, the applied voltage on SMA spring 1 is disconnected, and SMA spring 2 is activated. The pawl travels back by 5° and is now placed in contact with a different tooth, ready for the next rotation. The role of the compliant rod is to allow rotation in one direction only, i.e., only in the direction in actuator 1. When SMA actuator 2 is activated, the compliant rod's job is to hold the teethed disk in its place, preventing it from traveling back with the pawl. Throughout the movement of the pawl, the rubber band exerts a small inward force toward the center of the teethed disk to keep the pawl in contact with the teeth at all times. The mechanical stops are used to increase the precision of the mechanism, by bypassing the hysteresis behavior of Nitinol and the deployment of feedback control loops.

Since the components of the actuation system are in contact with the SMA wires that heat up, they need to have high-temperature resistance properties. PLA has low heat resistance; therefore, these components are 3-D-printed with "High Temp Resin V1" from Formlabs [34]. This material has the ability to resist temperature up to around 280 °C before deforming.

Based on the contraction speed of the SMA of about 0.2 s [37], the proposed antenna needs around 0.4 s for each 5° rotation. Such actuation speed fairs really well when compared with other mechanically reconfigurable antennas. For example, the actuation speed of a stepper motor in [35] requires around 150 ms, while pumps in [36] require around 1 min for actuation.

Although the actuation speed of the proposed prototype is lower than that of a traditional motor, the time needed to achieve the desired actuation is still fast enough for most applications, while avoiding the drawbacks of the large volume size and metallic nature of typical actuators. An additional advantage of the SMA actuator over the stepper motor is its low power consumption. A stepper motor such as in [35] requires around 800 mW of electric power compared with 300 mW for the SMA used in the proposed design herein.

Hence, major characteristics of the proposed design rely on its acceptable speed, precision, and low energy consumption. Such low energy requirement is also due to the lightweight rotation structure and the short time needed for contracting the SMA spring (less than 1 s). The other advantage of this system is the absence of metallic and magnetic parts as well as housings usually used in traditional motors. Finally, the mechanism is flexible in terms of the occupied volume and space. The SMA wires can be placed at different locations in the structure depending on the design constraints. Moreover, the shape of the SMA actuator can also be modified, for example, two straight wires (pseudo elastic effect) or flat springs (S-shaped).

III. Simulation and Measurement Results

As previously mentioned, mechanical reconfiguration is possible through placing two circular substrates, each consisting of a substrate and a copper layer, above a patch antenna. The separation distance between the copper layer and the driven antenna is optimized to 10 mm using ANSYS electronics desktop 2020 R1 [38]. Rotating one Moiré pattern with respect to the second fixed substrate creates a new grid

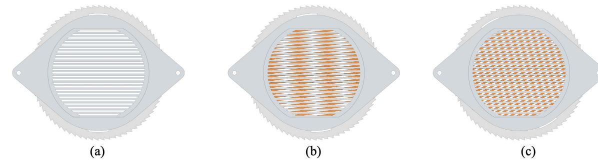

Fig. 9. Moiré patterns obtained by rotating two circular patches with a copper layer by (a) 0°, (b) 10°, and (c) 30°.

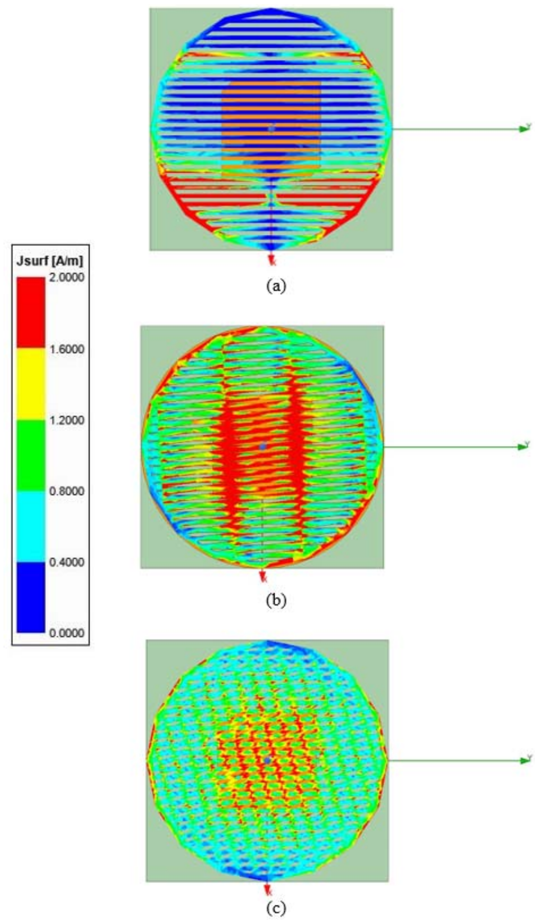

Fig. 10. Simulated surface current distribution on the Moiré patches at (a) 0° rotation, (b) 10° rotation, and (c) 30° rotation.

shape, resulting in almost vertical lines that are perpendicular to the original horizontal stripes as shown in Fig. 9. As the rotation angle is increased, the grid density increases, and the number of appearing vertical lines increases as shown in Fig. 9(c).

Although the rotation angles are of small increments, the major change in the resulting shape due to the Moiré phenomenon has a substantial effect on the antenna's radiation pattern. The surface current distributions presented in Fig. 10 give a clearer explanation on the polarization reconfiguration from linear vertical polarization at 0° rotation, to linear horizontal polarization at 10°, and to circular polarization (CP) at 30°. In Fig. 10(a), the maximum surface current on the Moiré patches is in the proximity of the radiating edges of the base antenna. These horizontal currents act as a reflector to most of the horizontal components of the traveling wave, hence resulting in a vertically polarized antenna.

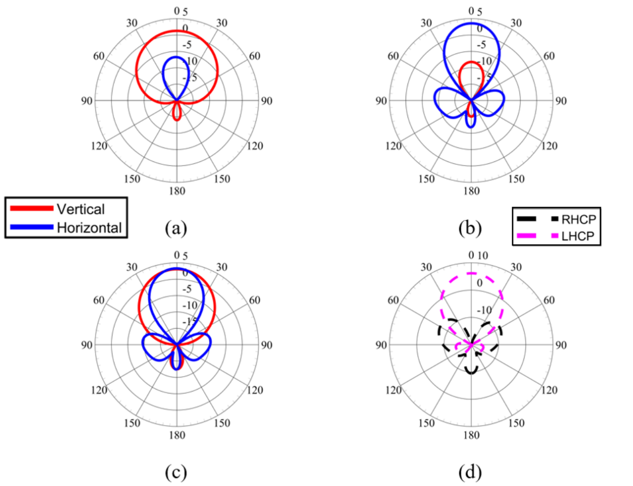

Fig. 11. Simulated radiation patterns. (a) Vertical and horizontal components of the antenna's radiation pattern at 0° rotation and at 2.5 GHz. (b) Vertical and horizontal components of the antenna's radiation pattern at 0° rotation and at 2.56 GHz. (c) Vertical and horizontal components of the antenna's radiation pattern at 30° rotation and at 2.56 GHz. (d) Co- an cross-polarization of the circularly polarized antenna radiation pattern at 30° rotation and at 2.56 GHz proving the antenna is left-hand circularly polarized.

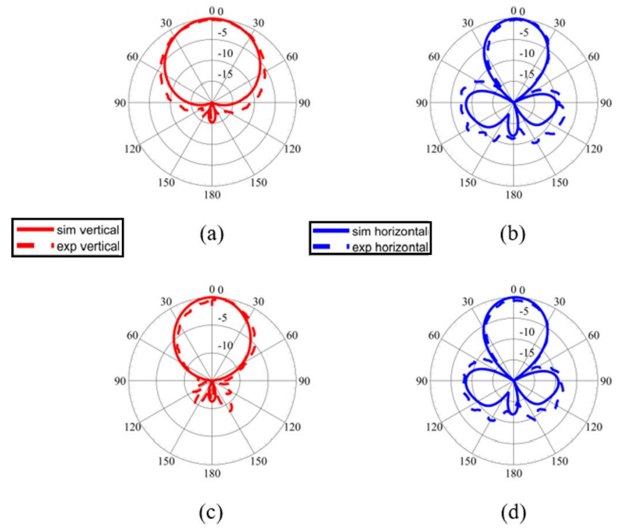

Fig. 12. Normalized simulated and measured radiation patterns of the dominant components at (a) 0° rotation at 2.50 GHz, (b) 10° rotation at 2.56 GHz, (c) vertical component of the circularly polarized pattern at 30° rotation and at 2.56 GHz, and (d) horizontal component of the circularly polarized pattern at 30° rotation and at 2.56 GHz.

At 10°, Fig. 10(b) indicates the existence of a similar situation; however, in this case, the current is maximal along the newly appearing vertical lines of the Moiré effect. The location of these vertical lines, near the edges of the antenna along its width, reflects most of the vertical components of the traveling wave, leading to a horizontally polarized antenna. At larger rotation angles, in particular at 30°, the high grid density allows for an even surface current throughout the copper layer, as seen in Fig. 10(c). This allows the traveling wave to have the same polarization as the driven antenna, that is, a left-handed circular polarization.

More interestingly, although polarization is still the same, the Moiré patches focus the beam and increase its directivity and gain. This can be observed from the total realized gain at different angles. The patch antenna alone exhibits a gain of 3.5 dB. Once the assembly and the actuation mechanism are installed, the gain is slightly decreased at 0° to 2.9 dB due to the effect of the assembly. The beam focusing effect is observed at 10° and 30°, where the beamwidth is reduced and the realized gain increases to 4.6 and 6.2 dB, respectively.

Fig. 11 depicts the vertical (gain θ) and horizontal (gain ϕ) components of the radiated beam. The antenna's radiation pattern measurement was obtained by positioning the antenna in an anechoic chamber. The antenna is distanced at 3.40 m from a horn antenna, at a height of 1.36 m. The antenna was rotated 360° on a turn table, and its radiation pattern was measured and recorded. The antenna's operation frequency for the various rotations of the Moiré pattern is measured using the Keysight PNA X [39].

The effect of the Moiré phenomenon, discussed using the surface current distributions, is apparent in these plots. At 0° and at 10°, Fig. 10(a) and (b) shows a different dominant co-polarization component with a cross-polarization isolation of around 10 dB, suggesting that the antenna polarization of the antenna can be considered linear with a vertical orientation at 0° and horizontal orientation at 10°. Fig. 10(c) indicates that at 30°, the peak gain of both the components is of similar magnitude, implying a circularly polarized wave. The resulting beam is LHCP, having the same handedness as the driven antenna. Fig. 11(a) and (b) shows the vertical and horizontal components of the linearly polarized radiation pattern at rotation angles of 0° and 10°, respectively. Fig. 11(c) shows the vertical and horizontal components of the radiation pattern, confirming its circularly polarized at 30° rotation. The co- and cross-polarization between RHCP and LHCP are shown in Fig. 11(d) where the proposed antenna is confirmed to be left-hand circularly polarized.

On the other hand, Fig. 12 reveals the good agreement between the simulated and experimental radiation patterns. As the antenna is vertically polarized at 0°, Fig. 12(a) presents the vertical component of the radiation pattern, whereas Fig. 12 (b) displays the horizontal component of the radiation pattern at 10°, since the antenna is horizontally polarized at that angle. Due to the circular polarization nature of the antenna at 30°, both the vertical and horizontal components have similar magnitudes, and therefore are shown in Fig. 12(c) and (d), respectively.

The directivity and the total realized gain of the presented work at the three states are pictured in Fig. 13. It can be observed that the beam becomes more directed as the rotation angle increases. The 3 dB beamwidth of the total realized gain decreases from 90° at 0° rotation angle, to 52° and 48° at the second and third states, respectively. As for the peak realized gain, it increases from around 3 dB at the first state, up to more than 5 dB at 30° rotation angle.

To better understand the LHCP state of the antenna, Fig. 14(a) and (b) shows the axial ratio of the reconfigurable antenna at 30° rotation angle, clearly demonstrating its circular

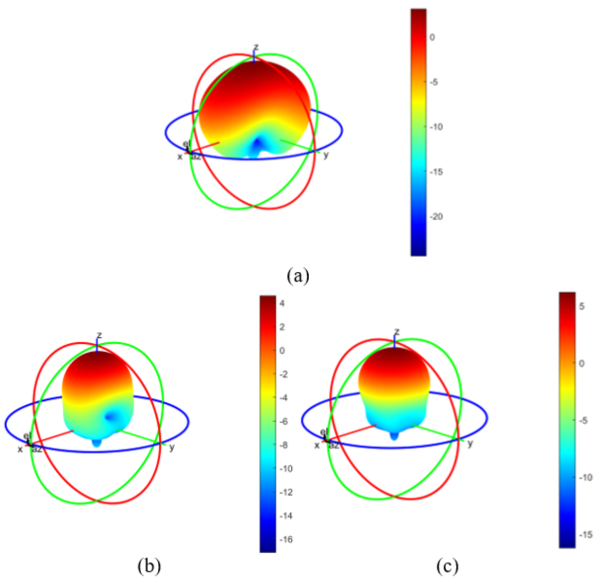

Fig. 13. Simulated radiation patterns at (a) 0° rotation at 2.5 GHz, (b) 10° rotation at 2.56 GHz, and (c) 30° rotation at 2.56 GHz.

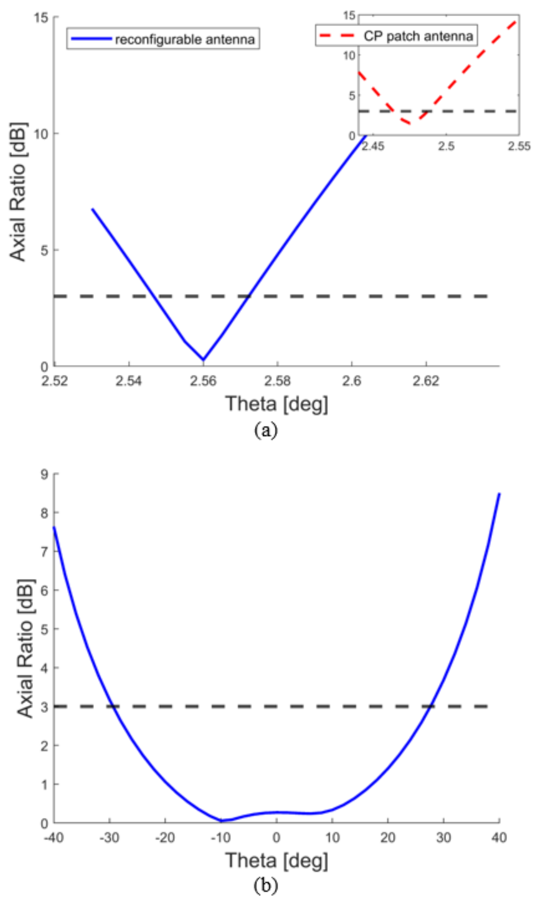

Fig. 14. Normalized simulated and measured radiation patterns of the dominant components at (a) 0° rotation at 2.50 GHz, (b) 10° rotation at 2.56 GHz, and (c) and (d) 30° rotation at 2.56 GHz.

polarization behavior. Interestingly, the axial ratio performance of the reconfigurable antenna is similar to that of the driven antenna, as shown in Fig. 14(a). As seen in (b), the radiated

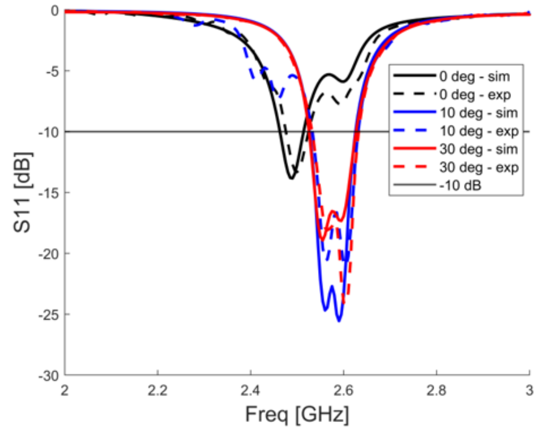

Fig. 15. Simulated and measured S11 of the proposed antenna.

TABLE I
REALIZED ROTATION (rot.) GAIN AND EFFICIENCY (eff.) ACROSS THE BANDWIDTH

Freq. [GHz]	0° rot. gain / eff.	10° rot. gain / eff.	30° rot. gain / eff.
2.48	2.8 dB (94%)	×	×
2.50	2.9 dB (96%)	×	×
2.52	2.9 dB (96%)	×	×
2.54	×	4.4 dB (91%)	×
2.55	×	4.6 dB (95%)	6.2 dB (96%)
2.56	×	4.5 dB (93%)	6.2 dB (96%)
2.57	×	3.8 dB (96%)	6.1 dB (94%)

beam displays circular polarization throughout its beamwidth of 48° (from −24° to +24°). As for the frequency response, Fig. 15 shows the comparison between the measured and simulated reflection coefficients (S_{11}) of the antenna for the different Moiré configuration. As the Moiré rotates from 0° to 10° and 30°, the antenna switches operation from 2.47–2.52 GHz to 2.53–2.63 GHz.

In Table I, the antenna's gain and efficiency are shown at different frequencies. In this table, each gain value is followed by its corresponding efficiency, and the "×" mark indicates that this frequency is out of the S_{11} bandwidth for the 0° and 10° rotations, and outside the CP range for the 30° rotation.

The proposed antenna has three modes of operation; when the actuator rotates between 0° and 10°, the frequency shifts but also its polarization shifts from linear vertical polarization into horizontal polarization. No common operating bandwidth is needed for this change in configurations. On the other hand, when the actuator rotates from 10° to 30°, a common operating bandwidth is achieved, and the operation frequencies remain the same but the polarization state shifts from linear vertical polarization to LHCP. Such features are important for various applications of the antenna. For example, in the case where this antenna is implemented on a satellite where satellite-to-satellite communication and space-to-earth communication necessitate a change in frequency and a change in polarization for various downlink and uplink needs.

The proposed antenna presents remarkable features that distinguish it from the works listed in Table II. First, the antenna is driven by SMA springs, not by volume occupying

TABLE II
COMPARISON WITH RECENT WORKS

Ref	[35]	[40]	[36]	Proposed Ant.
Antenna type	patch	patch array	dielectric resonator	patch
Reconfig. parameter	Pattern	Pattern	Pattern / Polarization	Frequency / Polarization / Directivity
Op. frequency	5.28 GHz	2.45 GHz	2.4 GHz	2.5 GHz
Volume	$3\lambda\times1.5\lambda\times0.6\lambda$	$2\lambda\times0.8\lambda\times1\lambda$	$1.6\lambda\times1.6\lambda\times0.2\lambda$	$\lambda\times\lambda\times0.1\lambda$
Actuator	stepper motor	manual	pumps	SMA actuator
Precise position control	active (stepper motor)	manual	active (feedback control)	Passive (ratchet & mech. stops)

pumps and dc motors. This, along with the need of only two planar substrates for the reconfiguration, makes the design noticeably compact. Second, the design is automated, not manual, yet it does not need any active position control, since the embedded ratchet mechanism and the mechanical stops are enough for positioning. Hence, the presented antenna along its inventive actuation mechanism is able to cater for dynamic communication needs whenever the need arises.

IV. CONCLUSION

In this article, the Moiré effect is leveraged to reconfigure the polarization state of an antenna. A low power, fast, and sturdy actuation mechanism that relies on a novel ratchet mechanism actuated using SMA helical springs is implemented for Moire' patterns' reconfiguration on top of a circularly polarized patch antenna. The change in Moire' patterns at small angle increments not only reconfigures the polarization schemes of the antenna but also reconfigures its gain for a more directive performance at various topologies. This mechanism makes this reconfigurable antenna perfectly suitable for implementation in satellite communication platforms.

ACKNOWLEDGMENT

The authors would like to thank the support of Dr. Fatima Asadallah and Hassan Shwaykani from the Antennas and RF Systems Laboratory, American University of Beirut, Beirut, Lebanon, for their help in the measurement of the prototype.

REFERENCES

[1] X. Liu, C. L. Zekios, and S. V. Georgakopoulos, "Analysis of a packable and tunable origami multi-radii helical antenna," *IEEE Access*, vol. 7, pp. 13003–13014, 2019.
[2] Y. Tawk, "Physically controlled CubeSat antennas with an adaptive frequency operation," *IEEE Antennas Wireless Propag. Lett.*, vol. 18, no. 9, pp. 1892–1896, Sep. 2019.
[3] L. H. Blumenschein, L. T. Gan, J. A. Fan, A. M. Okamura, and E. W. Hawkes, "A tip-extending soft robot enables reconfigurable and deployable antennas," *IEEE Robot. Autom. Lett.*, vol. 3, no. 2, pp. 949–956, Apr. 2018.
[4] I. T. Nassar, H. Tsang, D. Bardroff, C. P. Lusk, and T. M. Weller, "Mechanically reconfigurable, dual-band slot dipole antennas," *IEEE Trans. Antennas Propag.*, vol. 63, no. 7, pp. 3267–3271, Jul. 2015.
[5] H. L. Zhu, X. H. Liu, S. W. Cheung, and T. I. Yuk, "Frequency-reconfigurable antenna using metasurface," *IEEE Trans. Antennas Propag.*, vol. 62, no. 1, pp. 80–85, Jan. 2013.
[6] H. L. Zhu, S. W. Cheung, and T. I. Yuk, "Mechanically pattern reconfigurable antenna using metasurface," *IET Microw., Antennas. Propag.*, vol. 9, no. 12, pp. 1331–1336, Jun. 2015.
[7] Q. Tang *et al.*, "Flat-panel mechanical beam steerable array antennas with in-plane rotations: Theory, design and low-cost implementation," *IEEE Open J. Antennas Propag.*, vol. 2, pp. 679–688, 2021.
[8] D. Rodrigo, L. Jofre, and B. A. Cetiner, "Circular beam-steering reconfigurable antenna with liquid metal parasitics," *IEEE Trans. Antennas Propag.*, vol. 60, no. 4, pp. 1796–1802, Apr. 2012.
[9] A. Mehdipour, T. A. Denidni, A.-R. Sebak, C. W. Trueman, I. D. Rosca, and S. V. Hoa, "Mechanically reconfigurable antennas using an anisotropic carbon-fibre composite ground," *IET Microw., Antennas Propag.*, vol. 7, no. 13, pp. 1055–1063, Oct. 2013.
[10] A. Boukarkar, X. Q. Lin, Y. Jiang, Y. J. Chen, L. Y. Nie, and P. Mei, "Compact mechanically frequency and pattern reconfigurable patch antenna," *IET Microw., Antennas Propag.*, vol. 12, no. 11, pp. 1864–1869, 2018.
[11] I. T. McMichael, "A mechanically reconfigurable patch antenna with polarization diversity," *IEEE Antennas Wireless Propag. Lett.*, vol. 17, no. 7, pp. 1186–1189, Jul. 2018.
[12] R. Pereira, R. Gillard, R. Sauleau, P. Potier, T. Dousset, and X. Delestre, "Dual linearly-polarized unit-cells with nearly 2-bit resolution for reflectarray applications in X-band," *IEEE Trans. Antennas Propag.*, vol. 60, no. 12, pp. 6042–6048, Dec. 2012.
[13] H. F. Abutarboush *et al.*, "A reconfigurable wideband and multiband antenna using dual-patch elements for compact wireless devices," *IEEE Trans. Antennas Propag.*, vol. 60, no. 1, pp. 36–43, Jan. 2011.
[14] M. Riel and J.-J. Laurin, "Design of an electronically beam scanning reflectarray using aperture-coupled elements," *IEEE Trans. Antennas Propag.*, vol. 55, no. 5, pp. 1260–1266, May 2007.
[15] M. A. Forman and Z. B. Popovic, "A tunable second-resonance cross-slot antenna," in *Proc. IEEE Antennas Propag. Soc. Int. Symp.*, vol. 1, Jul. 1997, pp. 18–21.
[16] P.-L. Chi, R. Waterhouse, and T. Itoh, "Compact and tunable slot-loop antenna," *IEEE Trans. Antennas Propag.*, vol. 59, no. 4, pp. 1394–1397, Apr. 2011.
[17] T. Debogovic and J. Perruisseau-Carrier, "Low loss MEMS-reconfigurable 1-bit reflectarray cell with dual-linear polarization," *IEEE Trans. Antennas Propag.*, vol. 62, no. 10, pp. 5055–5060, Oct. 2014.
[18] J. M. Kovitz, H. Rajagopalan, and Y. Rahmat-Samii, "Design and implementation of broadband MEMS RHCP/LHCP reconfigurable arrays using rotated E-shaped patch elements," *IEEE Trans. Antennas Propag.*, vol. 63, no. 6, pp. 2497–2507, Jun. 2015.
[19] B. Majumder, K. Krishnamoorthy, J. Mukherjee, and K. P. Ray, "Frequency-reconfigurable slot antenna enabled by thin anisotropic double layer metasurfaces," *IEEE Trans. Antennas Propag.*, vol. 64, no. 4, pp. 1218–1225, Apr. 2016.
[20] Y. Tawk, J. Costantine, F. Ayoub, C. Christodoulou, D. Doyle, and S. Lane, "Physically reconfigurable antennas: Concepts and automation," in *Proc. IEEE Int. Symp. Antennas Propag. USNC/URSI Nat. Radio Sci. Meeting*, Jul. 2017, pp. 419–420.
[21] I. T. Nassar, T. M. Weller, and C. P. Lusk, "Radiating shape-shifting surface based on a planar Hoberman mechanism," *IEEE Trans. Antennas Propag.*, vol. 61, no. 5, pp. 2861–2864, May 2013.
[22] X. Yang *et al.*, "A mechanically reconfigurable reflectarray with slotted patches of tunable height," *IEEE Antennas Wireless Propag. Lett.*, vol. 17, no. 4, pp. 555–558, Apr. 2018.
[23] S. J. Mazlouman, A. Mahanfar, C. Menon, and R. G. Vaughan, "Reconfigurable axial-mode helix antennas using shape memory alloys," *IEEE Trans. Antennas Propag.*, vol. 59, no. 4, pp. 1070–1077, Apr. 2011.
[24] J. T. Bernhard, E. Kiely, and G. Washington, "A smart mechanically actuated two-layer electromagnetically coupled microstrip antenna with variable frequency, bandwidth, and antenna gain," *IEEE Trans. Antennas Propag.*, vol. 49, no. 4, pp. 597–601, Apr. 2001.
[25] E. Gabrielyan, "The basics of line moiré patterns and optical speedup," Mar. 2007, p. 9, *arXiv:physics/0703098*.
[26] F.-P. Chiang, "Moiré methods of strain analysis," *Experim. Mech.*, vol. 19, no. 8, pp. 290–308, 1979.
[27] V. J. Cadarso, S. Chosson, K. Sidler, R. D. Hersch, and J. Brugger, "High-resolution 1d moirés as counterfeit security features," *Light, Sci. Appl.*, vol. 2, no. 7, p. 86, 2013.
[28] J. C. Booth, M. Whiley, C. Rudd, and M. Kranz, "Material database for additive manufacturing techniques," AMRDEC Redstone Arsenal United States, 2017.

[29] D. J. Leo, *Engineering Analysis of Smart Material Systems*. Hoboken, NJ, USA: Wiley, 2007.
[30] J. A. Guadalupe, D. Copaci, D. S. del Cerro, L. Moreno, and D. Blanco, "Efficiency analysis of SMA-based actuators: Possibilities of configuration according to the application," *Actuators*, vol. 10, no. 3, p. 63, Mar. 2021.
[31] K. M. Jani, "Design optimisation of shape memory alloy linear actuator applications" RMIT Univ., 2016.
[32] S. Mahdavi and P. J. Bentley, "Evolving noise tolerant antenna configurations, using shape memory alloys," in *Proc. 2nd Int. Conf. Comp. Intel., Robotics Auton. Syst. (CIRAS)*, 2003, pp. 1–6.
[33] P. Motzki, "Efficient SMA actuation—Design and control concepts," in *Proc. 1st Int. Electron. Conf. Actuator Technol., Mater., Devices Appl.*, Nov. 2020, pp. 1–9.
[34] *Using High Temp Resin*, Formlabs, Somerville, MA, USA, 2022.
[35] F. A. Asadallah *et al.*, "An antenna system with a voice-controlled personalized switchable radiation coverage," *IEEE Antennas Wireless Propag. Lett.*, vol. 17, no. 4, pp. 693–696, Apr. 2018.
[36] J. Ren *et al.*, "Radiation pattern and polarization reconfigurable antenna using dielectric liquid," *IEEE Trans. Antennas Propag.*, vol. 68, no. 12, pp. 8174–8179, Dec. 2020.
[37] H. Y. Teh, "Fast, accurate force and position control of shape memory alloy actuators," Tech. Rep., 2008.
[38] *ANSYS HFSS*, ANSYS, Canonsburg, PA, USA, 2020.
[39] (2021). Keysight. *PNA-X Network Analyzers*. [Online]. Available: https://www.keysight.com/zz/en/products/network-analyzers/pna-network-analyzers/pna-x-network-analyzers.html
[40] M. Hamza, C. L. Zekios, and S. V. Georgakopoulos, "A thick origami reconfigurable and packable patch array with enhanced beam steering," *IEEE Trans. Antennas Propag.*, vol. 68, no. 5, pp. 3633–3653, Jan. 2020.

Joe Taoum received the B.E. and M.E. degrees in mechanical engineering from the American University of Beirut, Beirut, Lebanon, in 2014 and 2019, respectively.

His current research focuses on mechanically reconfigurable structures and on antenna's reconfigurations.

Elie Shammas (Senior Member, IEEE) received the B.E. degree from the Mechanical Engineering Department, American University of Beirut, Beirut, Lebanon, in 1999, and the Ph.D. degree from the Mechanical Engineering Department, Carnegie Mellon University, Pittsburgh, PA, USA, in March 2006.

After three years, he was a Research and Development Engineer with Hexagon Metrology, Oceanside, CA, USA, working on developing calibration algorithms for portable coordinate measuring machines. He joined the Mechanical Engineering Department, American University of Beirut, in 2010, where he is currently an Associate Professor. His research expertise spans multiple disciplines, such as robotic joints, mobile robotic platforms, and medical devices design; nonholonomic and optimal motion planning; and kinematic calibration of robotic manipulators.

Joseph Costantine (Senior Member, IEEE) received the bachelor's degree from the Second Branch of the Faculty of Engineering, Lebanese University, Beirut, Lebanon, in 2004, the M.E. degree from the American University of Beirut, Beirut, in 2006, and the Ph.D. degree from the University of New Mexico, Albuquerque, NM, USA, in 2009.

He is currently an Associate Professor with the Electrical and Computer Engineering Department, American University of Beirut, and a World Economic Forum Young Scientist. He has 11 provisional and full U.S. patents. He has published so far two books, one book chapter, and more than 160 journal articles and conference papers. His research interests include reconfigurable antennas, cognitive radio, RF energy harvesting systems, antennas and rectennas for internet of things (IoT) devices, RF systems for biomedical devices, wireless characterization of dielectric material, and deployable antennas for small satellites.

Dr. Costantine has been an Associate Editor of the IEEE ANTENNAS AND WIRELESS PROPAGATION LETTERS since July 2018. He received many awards and honors throughout his career including the 2008 IEEE Albuquerque Chapter Outstanding Graduate Award, the three year (2011–2013) Summer Faculty Fellowship with Kirtland's Space Vehicles Directorate in NM, USA, the 2017 first prize at the Idea-thon of International Healthcare Industry Forum, the 2019 Excellence in Teaching Award from American University of Beirut, the 2018 and 2020 Science and Technology Corporation (STC) Science and Technology Innovation Awards, and the 2020 Distinguished Young Alumni Award from the School of Engineering, University of New Mexico.